



This is a repository copy of *Molecular Engineering of Conjugated Polymers for Efficient Hole Transport and Defect Passivation in Perovskite Solar Cells*.

White Rose Research Online URL for this paper:
<http://eprints.whiterose.ac.uk/125594/>

Version: Accepted Version

Article:

Cai, F., Cai, J., Yang, L. et al. (6 more authors) (2018) Molecular Engineering of Conjugated Polymers for Efficient Hole Transport and Defect Passivation in Perovskite Solar Cells. *Nano Energy*, 45. pp. 28-36. ISSN 2211-2855

<https://doi.org/10.1016/j.nanoen.2017.12.028>

Reuse

This article is distributed under the terms of the Creative Commons Attribution-NonCommercial-NoDerivs (CC BY-NC-ND) licence. This licence only allows you to download this work and share it with others as long as you credit the authors, but you can't change the article in any way or use it commercially. More information and the full terms of the licence here: <https://creativecommons.org/licenses/>

Takedown

If you consider content in White Rose Research Online to be in breach of UK law, please notify us by emailing eprints@whiterose.ac.uk including the URL of the record and the reason for the withdrawal request.



eprints@whiterose.ac.uk
<https://eprints.whiterose.ac.uk/>

Molecular Engineering of Conjugated Polymers for Efficient Hole Transport and Defect Passivation in Perovskite Solar Cells

Feilong Cai^{1,2}, Jinlong Cai^{1,2}, Liyan Yang^{1,2}, Wei Li^{1,2}, Robert S. Gurney^{1,2}, Hunan Yi³, Ahmed Iraqi³, Dan Liu^{1,2}, Tao Wang^{1,2*}

¹School of Materials Science and Engineering, Wuhan University of Technology, Wuhan, 430070, China * E-mail: twang@whut.edu.cn

²State Key Laboratory of Silicate Materials for Architectures, Wuhan University of Technology, Wuhan, 430070, China

³Department of Chemistry, University of Sheffield, Sheffield, S3 7HF, UK

Organic-inorganic hybrid perovskite solar cells represent an exceptional candidate for next-generation photovoltaic technology. However, the presence of surface defects in perovskite crystals limits the performance as well as the stability of perovskite solar cells. We have employed a series of carbazole and benzothiadiazole (BT) based donor-acceptor copolymers, which have different lengths of alkoxy side-chains grafted on the BT unit, as the dopant-free hole transport materials (HTMs) for perovskite solar cells. We demonstrate that although these side-chains can reduce the π - π stacking structural order of these copolymers to affect the hole transport properties, the methoxy unit introduces a desired defect passivation effect. Compared to the Spiro-OMeTAD-based device, the copolymer with methoxy side-chains on the BT unit (namely PCDTBT1) as the HTM achieved superior power conversion efficiency and stability due to efficient hole transport and the suppression of trap-induced degradation, whilst the copolymer with octyloxy side-chains on the BT unit (namely PCDTBT8) as the HTM lead to poor performance and stability.

Keywords

Perovskite solar cells, hole transport, defect passivation, conjugated polymer

1. Introduction

Organic-inorganic hybrid perovskite solar cells (PSCs) have attracted extensive research interest due to their efficient light harvesting capability over a broad wavelength region, high defect tolerance with a tunable band gap, and their simple solution fabrication process using low cost materials^[1-3]. PSCs have achieved an impressive improvement in power conversion efficiency (PCE) from the initial 3.8%^[4] to 22.1%^[5] through composition engineering^[6,7], charge transport layer design^[8,9] and interface modification^[10,11] in the past few years.

Planar heterojunction PSCs that are made by stacking various planar thin films together are easy to fabricate, and have been implemented in two types of device configurations, namely inverted (p-i-n) and directed (n-i-p) structures. For the latter architecture, the hole transport materials (HTMs) are deposited on top of the perovskite photoactive layer, which plays a crucial role for charge extraction and environmental stabilization^[12]. The most widely used HTM is the small molecule 2,2',7,7'-tetrakis(*N,N*-di-*p*-methoxyphenylamine)-9,9'-spirobifluorene (Spiro-OMeTAD) which has enabled high efficiency PSCs over 20%^[13-15]. However, this material has high resistivity and thus requires p-doping with an indispensable combination of integrated additives bis(trifluoromethane)sulfonimide lithium salt(Li-TFSI) and 4-tert-butylpyridine (TBP) to overcome this limitation^[16,17], whereas Li-TFSI has strong water absorption tendency and TBP can corrode the perovskite material^[18]. Furthermore, the doped Spiro-OMeTAD film needs to be exposed to ambient conditions for a long-term oxidation process to gain good hole-transport properties^[19], with the extrinsic environmental conditions (e.g. O₂, H₂O, temperature, and light) needing to be well controlled to avoid any degradation of the Spiro-OMeTAD and the underlying perovskite layers. The use of dopants to increase the electrical properties is believed to be a trade-off with stability due to potential diffusion of small molecules during long-term device operation. The complex doping process also presents difficulties for large-scale production, which makes the material commercially unfavorable.

In addition to the manipulation of electronic properties to ensure efficient hole transport, the top HTM layer should also ideally be designed to enable the passivation of various trap sites on the crystal surface and at the grain boundaries of perovskite to minimize the non-radiative charge recombination. These defects include halide vacancies, as well as the PbI₂ species that are generated either by incomplete conversion of precursors or from partial decomposition of perovskite during the processing steps, for example thermal annealing, due to its low thermal stability^[20]. These under-coordinated Pb atoms can act as recombination centers leading to a severe accumulation of charges at the contacts^[21,22], which need to be passivated through binding to electron-rich Lewis bases. Surface treatment of perovskite films using organic Lewis bases containing thiophene^[23], pyridine^[24] and amine groups^[25] or introducing the Lewis base 1,1-dicyanomethylene-3-indanone

with n-type semiconductor properties as electron transport layers^[26] have all been shown to endow significant enhancement of device performance. Therefore, it is paramount to prepare pristine HTMs without doping additives that can achieve effective charge extraction, moisture resistance as well as trap passivation. Inorganic materials such as copper thiocyanate (CuSCN)^[27], copper iodide (CuI)^[28] and copper phthalocyanine (CuPc)^[29] can deliver appreciable incremental improvements, however these improvements in efficiency are still unable to rival those achieved using doped-Spiro-MeOTAD layers in devices.

Previous work has demonstrated that structural design of small organic molecules and conjugated polymers can impart special features^[30,31], for example built-in field^[32], molecular orientation^[33] and interfacial coupling^[34], which can improve the charge-transport property to serve as efficient HTMs in PSCs. Herein, we introduce three carbazole and benzothiadiazole (BT) based donor-acceptor (D-A) copolymers poly[N-9'-heptadecanyl-2,7-carbazole-*alt*-5,5-(4',7'-di-2-thienyl-2',1',3'-benzothiadiazole)] (PCDTBT), poly[9-(heptadecan-9-yl)-9H-carbazole-2,7-diyl-*alt*-(5,6-bis(methoxy)-4,7-di(thiophen-2-yl) benzo[c][1,2,5] thiadiazole-5,5-diyl] (PCDTBT1) and poly[9-(heptadecan-9-yl)-9H-carbazole-2,7-diyl-*alt*-(5,6-bis-(octyloxy)-4,7-di(thiophen-2-yl)benzo[c][1,2,5]thiadiazole)-5,5-diyl] (PCDTBT8) as HTMs without any doping additives. The PCDTBT macromolecules can pack together through π - π interactions, enabling relatively high charge transfer in the vertical direction from the perovskite to the HTM layer. The synergistic passivation effect of thiophene units and methoxy side-chains with the presence of π - π order in PCDTBT1 can effectively reduce trap sites on the perovskite film surface, leading to a maximum PCE of 19.1% in the derived planar heterojunction PSCs, which is comparable with the doped spiro-OMeTAD based devices, while achieving improved device stability.

2. Results and Discussion

We fabricated planar heterojunction PSCs employing the structure of glass/ITO/TiO₂/PC₆₀BM/MAPbI₃/HTMs/MoO₃/Au as shown in Fig. 1a, using PCDTBT, PCDTBT1, and PCDTBT8 as the HTMs respectively, and compared their photovoltaic performance with that of the doped-spiro-OMeTAD based device. The electron transport material (ETM) here employed our previously synthesized TiO₂ via a low-temperature route^[35]. It was further modified using titanium oxide bis(2,4-pentanedionate) (TOPD) as the binder to reduce morphological defects between TiO₂ nanoparticles. This TiO₂:TOPD complex has been demonstrated as an efficient ETM to prepare high performing PSCs.^[35] The conjugated copolymers PCDTBT, PCDTBT1, PCDTBT8 were synthesized in our previous work^[36,37]. Fig. 1(c) illustrates their chemical structure, which comprise a carbazole donor moiety, flanked by two thienyl groups that are co-polymerized with a BT unit. This BT unit itself is functionalized with two methoxy or octyloxy substituents, resulting

in copolymers named PCDTBT1 and PCDTBT8 respectively. The alkoxy group can improve the solubility of conjugated polymers, as well as affecting the electronic, photophysical and photovoltaic properties, which have been verified in organic solar cells^[36,37]. The UV-vis absorptions of these conjugated polymers are shown in Fig. S1a (Supporting information), the maximum absorption peaks (λ_{max}) of PCDTBT, PCDTBT1 and PCDTBT8 are centered at 572, 544 and 538 nm respectively. It should also be noted that the onset point (λ_{onset}) is blueshifted to lower wavelengths when grafting alkoxy side-chains on the BT unit. This can be further demonstrated through the photoluminescence (PL) spectra of the three polymer thin films shown in Fig. S1b (Supporting information), exhibiting an obvious blueshift of emission peaks for the polymers with alkoxy side-chains in comparison to those of pristine PCDTBT without any substituents on the BT unit.

The density functional theory (DFT) method and Gaussian 09 package were used to further understand the electronic structure of these conjugated polymers, which we present in Fig. 1d and Fig. S2 (Supporting information). Fig. 1d shows electrostatic potential (ESP) distribution of these polymers, showing negative ESP concentration on the π -conjugated main chain and O atoms. Compared to the pristine PCDTBT, the introduction of alkoxy side-chains disrupts the conjugation between the “donor” and the “acceptor” moieties in PCDTBT, which can be speculated from the discontinuous negative ESP in the main chain. The three dihedral angles between different parts of polymers (Fig. S2, Supporting information) can quantitatively measure the steric hindrance effect of alkoxy side-chains, which will eventually impact the co-planarity of these conjugated polymers. Table 1 summarizes values of these dihedral angles, with PCDTBT presenting the greatest co-planarity of all participating aromatic units and PCDTBT8 showing a severely broken co-planarity with the largest torsional angles (see Fig. 1d). The influences of charge polarization and co-planarity of these conjugated polymers on device performance will be discussed in the following section.

As shown in the Fig. S2 (Supporting information), the HOMOs (highest occupied molecular orbitals) of these polymers are mainly located on the conjugated backbone of polymers, and the LUMOs (lowest unoccupied molecular orbitals) are essentially located on the BT unit. The preliminary calculation results show that the introduction of side-chains mainly affect the bandgap through changing the LUMOs, while the HOMOs are fairly similar, thus leading to the significant difference in optical properties. The energy level diagrams of PSCs in this work are depicted in Fig. 1b, the HOMO levels of three polymers are around -5.4 eV^[36,38], slightly lower than that of spiro-OMeTAD (~ -5.2 eV), suggesting a more favorable band alignment with the valence band edge of the perovskite, which in principle will reduce the energy loss during charge extraction and transportation in PSCs.

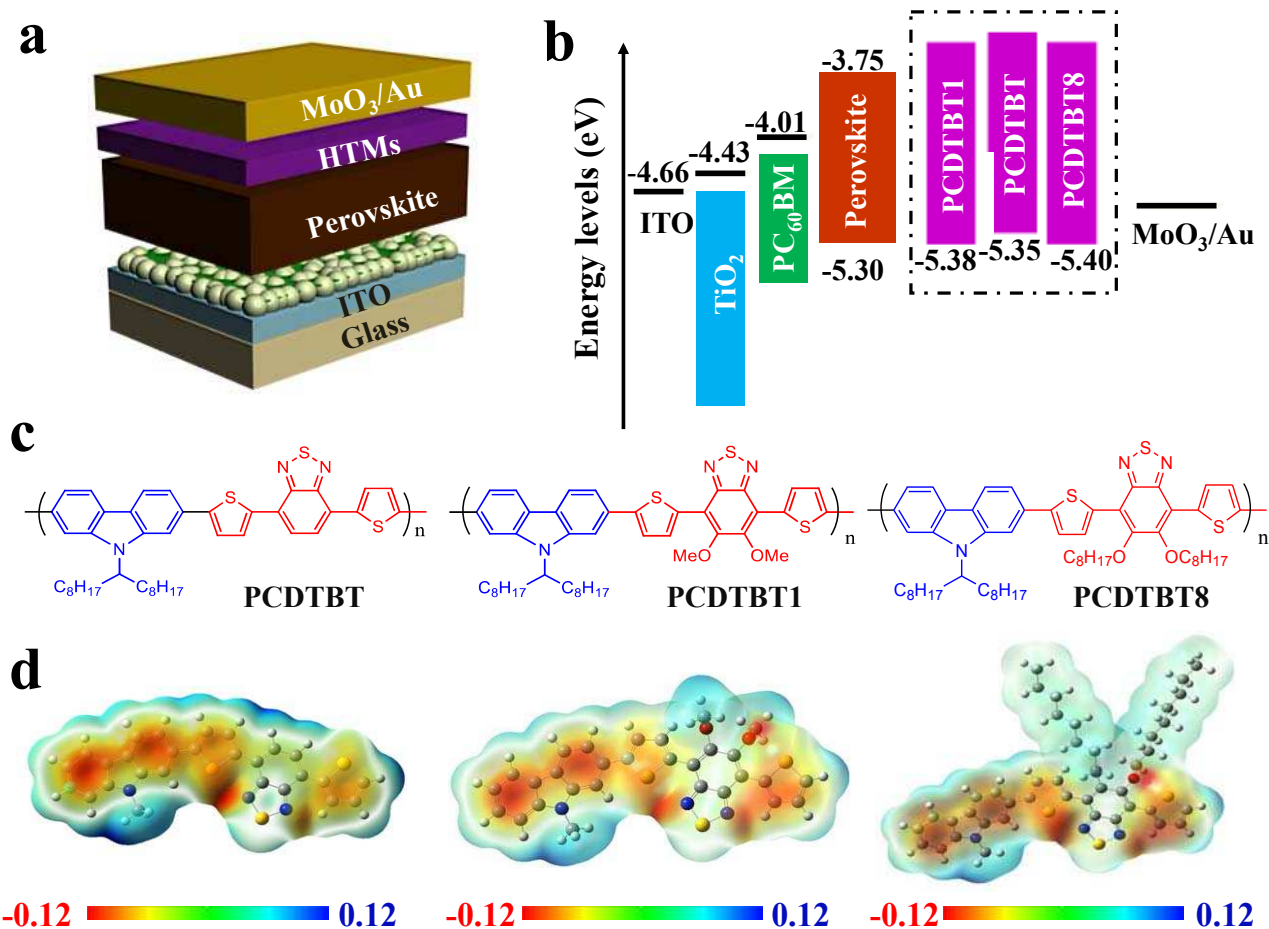


Fig. 1. (a) Schematic structure and (b) energy-level diagram of the PSCs. (c) The molecular structure and (d) computed ESP profiles of PCDTBT, PCDTBT1 and PCDTBT8. Quantitative values of electrostatic potentials are in au.

Table 1. Calculated dihedral angles of polymers.^a

Polymers	Dihedral angle 1 (degrees)	Dihedral angle 2 (degrees)	Dihedral angle 3(degrees)
PCDTBT	0.08	0.07	0.05
PCDTBT1	25.54	16.62	9.52
PCDTBT8	26.71	21.18	11.59

^a Calculations were carried out for one repeating unit of each polymer, in gas phase, at the temperature of 0 K and in vacuum.

Optimization of the HTM layer in our PSCs suggests that the optimum thickness of these conjugated copolymers is around 20 nm, being significantly thinner than the *ca.* 200 nm for the spiro-OMeTAD HTM. The surface morphology of perovskite, perovskite/PCDTBT1, and perovskite/spiro-OMeTAD films was analyzed by scanning probe microscope (SPM), as shown in Fig. S3 (Supporting information). We observe that the thin PCDTBT1 film can decrease the root-mean-square (RMS) surface roughness from 11.3 to 9.8 nm, and help to reduce the contact resistance. In the meantime, it shows a uniform coverage on the perovskite from the phase image

although the perovskite crystal profile can still be visible from the height image. For the perovskite film capped with the much thicker spiro-OMeTAD film, we see uniformly distributed white dots that can be attributed to the dopants within the film.

We found that the device performance depends on the chemical structure of the conjugated polymer HTMs. The best-performing J - V curves of devices using the three different HTMs are presented in Fig. 2a and their corresponding average statistics are listed in Table 2. The device using PCDTBT as the HTM can achieve a decent PCE of 17.1%. When PCDTBT1 with two methoxy units on the BT unit was employed as the HTM, the champion device efficiency was substantially improved to 19.1%, with the values of J_{sc} , V_{oc} and FF as 22.2 mA/cm², 1.1 V and 78.2% respectively, which were comparable with the reference device using doped-spiro-OMeTAD as HTM. However, the PCDTBT8-based device can only obtain a PCE of around 15%, with such a significant difference mainly attributed to the reduced V_{oc} and FF, whilst the reduction of J_{sc} was marginal. Additionally, Fig. 2b shows the steady-state PCEs at an external bias close to the maximum power points (MPP) of 17.0, 19.0 and 15.1% for the three HTMs respectively, values that are consistent with our J - V sweep measurements. With regard to the notorious hysteresis of PSCs that has been commonly reported in the literature^[39,40], the device J - V curves under reverse and forward scans are shown in the Fig. S4 (Supporting information), demonstrating negligible hysteresis or discrepancy of photovoltaic parameters. Moreover, by changing the voltage scan rate through regulating the step size and voltage setting time during the testing procedure, we observe that the J - V curves show an excellent degree of consistency under different scan rates and delay times^[41] (see Figure S5, Supporting information). The external quantum efficiency (EQE) curves of these PSCs are presented in Fig. 2c, which shows high EQE values in the visible spectrum, and the integration of the EQE spectra yields a J_{sc} for all systems of around 21.5 mA/cm², close to the J_{sc} obtained from J - V scans, confirming the accuracy of our device efficiency characterizations. In addition, Fig. 2d shows that each group has a narrow distribution of efficiency, exhibiting outstanding reproducibility of devices owing to excellent stability of the sole conjugated polymer without dopants as the HTM. We have also fabricated a batch of devices with larger active area of 4 mm², and the device metrics are summarized in Table S1. With the increased active area from 2.12 to 4 mm², the device metrics values decreased slightly due to the increased series resistance whilst the PCE values remained essentially unchanged ascribed to the exceptional charge transport properties of perovskite. An encouraging PCE of 18.9%, with a V_{oc} of 1.09 V, J_{sc} of 22.3 mA cm⁻² and FF of 77.6%, was achieved for the device using PCDTBT1 as HTM, illustrating that the PCDTBT1-based PSCs has the potential to fabricate large-area high-performing devices. This weak PCE dependence on the size of the active area of perovskite solar cells is significantly different with that of polymer solar cells which show strong size-dependence.^[42]

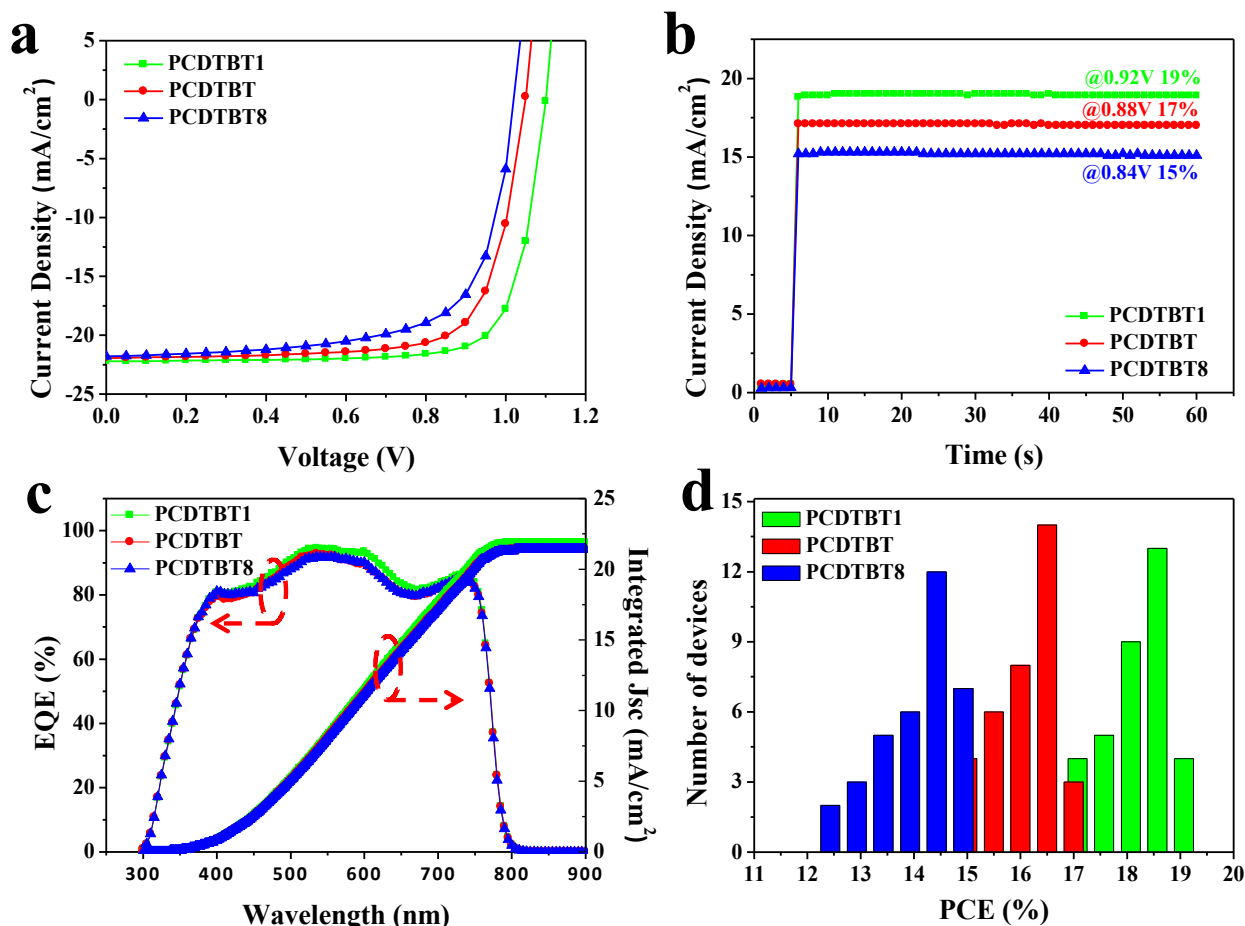


Fig. 2. (a) J - V curves of the optimized devices with different HTMs and (b) their corresponding steady-state power output at the maximum power point. (c) EQE spectra and the integrated current densities. (d) Histograms of device PCE generated from 35 devices of each set.

Table 2. Device metrics parameters of perovskite solar cells employing different HTMs.

HTMs	Scan direction	V_{oc} (V)	FF	J_{sc} (mA cm ⁻²)	PCE _{ave} (PCE _{max})
PCDTBT	RS	1.05±0.01	72.34±1.25	-21.62±0.28	16.43±0.47(17.1)
	FS	1.05±0.01	71.45±1.42	-21.58±0.34	16.14±0.38(16.9)
PCDTBT1	RS	1.10±0.01	77.63±1.23	-21.78±0.33	18.67±0.44(19.1)
	FS	1.10±0.01	76.14±0.71	-21.81±0.36	18.26±0.31(18.8)
PCDTBT8	RS	1.02±0.01	67.31±0.92	-21.29±0.31	14.81±0.47(15.4)
	FS	1.02±0.01	66.52±1.12	-21.18±0.35	14.67±0.36(15.1)
Spiro-OMeTAD	RS	1.09±0.01	78.91±1.32	-22.24±0.36	18.81±0.63(19.4)
	FS	1.08±0.01	76.68±1.26	-22.17±0.43	18.45±0.84(18.8)

V_{oc} , open circuit voltage; FF, fill factor; J_{sc} , short-circuit current density; PCE, power conversion efficiency. Average performance parameters and their S.D. were obtained based on 20 cells for each set.

We proceed to illustrate how the molecular structure of the three conjugated polymers used in this work could affect the charge transportation and recombination within devices that consequently determine the efficiency via their impact on V_{oc} and FF . We first explored the charge extraction efficiency of perovskite devices at various interfaces when incorporating different HTMs using

steady-state and time-resolved photoluminescence (PL) measurements. As can be seen from Fig. 3a, the bi-layered perovskite/HTM thin films showed a significant reduction of PL intensity with respect to that of the pristine perovskite film, which can be associated with sufficient hole injection from perovskite to HTMs^[43]. The shoulder peaks appearing at *ca.* 600 nm stemmed from the emission peaks of the conjugated polymers. The perovskite/PCDTBT bilayer shows the most efficient interfacial charge transfer, given that it has the highest extent of PL quenching among the three bilayer systems. The introduction of alkoxy side-chains seems to impede the charge extraction, with PL intensity of the perovskite/PCDTBT8 bilayer remaining as the highest due to the worst quenching yield of perovskite. The differing charge transport from perovskite to HTM in these systems can be explained by the different levels of structural order existing in the HTM layers. As mentioned above, PCDTBT chains retain complete conjugation of all units, thereby solution-cast PCDTBT films form face-on intramolecular π - π stacks although they are largely in an amorphous state without forming crystalline domains^[44,45]. These perpendicularly packed HTM molecules on the perovskite surface will facilitate the vertical hole transportation from perovskite to the HTM layer^[46]. The spatial steric hindrance of the alkoxy substituents on the BT units of the conjugated backbones of PCDTBT1 and PCDTBT8 reduces the co-planarity and the π - π stacking structure which leads to a deterioration of charge transport from perovskite to HTMs. This negative effect is less pronounced when the length of the alkoxy side-chain is short (e.g. PCDTBT1), but will significantly disrupt the π - π stacks and reduce charge transport when the side-chains are long^[47,48]. Consequently, the large size of octyloxy groups within the PCDTBT8 chains will lead to the worst co-planarity amongst this series of polymers and the least π - π stacking between polymer chains, therefore the lowest hole transfer efficiency. This is also confirmed by the time-resolved PL measurements. Carrier decay lifetimes were obtained by fitting the PL decaying curves in Fig. 3b through an exponential diffusion model. The average lifetime reduced from 138 ns for the pristine perovskite film to 2.1, 50.8, and 81.8 ns respectively when applying a PCDTBT, PCDTBT1 or PCDTBT8 layer on top. The reduced decay lifetime affirms the critical function of ordered π - π stacking, providing a rapid pathway for hole transport.

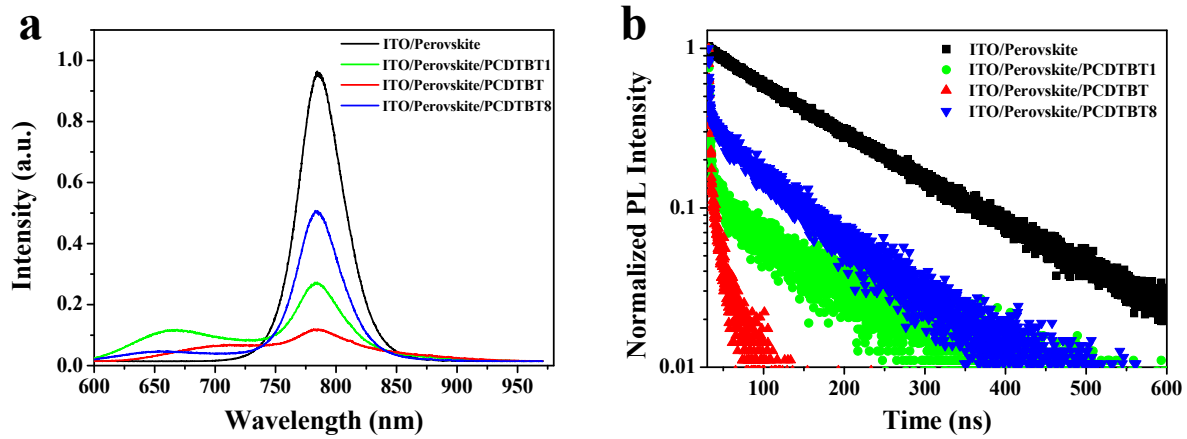


Fig. 3. (a) Steady-state and (b) time-resolved photoluminescence spectra of ITO/perovskite, ITO/perovskite/PCDTBT1, ITO/perovskite/PCDTBT and ITO/perovskite/PCDTBT8, respectively.

Although the above investigation suggests that the charge transport at the perovskite/PCDTBT1 interface is not the most efficient, device studies presented in Fig. 2 and Table 2 show that it is a superior HTM among all three copolymers, suggesting that interfacial charge transport is not the sole factor that will determine device efficiency. To understand this disagreement between charge transport and device efficiency, we further investigated the charge-carrier dynamics of perovskite solar cells. First, we conducted dark-current measurements to study the leakage current from carrier recombination in the devices. As shown in Fig. 4a, the dark current density of the PCDTBT1-based device is almost several orders of magnitude lower than those using PCDTBT and PCDTBT8 as HTMs, indicating that more photocurrent will flow through the device and therefore reduced charge recombination^[49,50]. This is also demonstrated from their light ideality factors under illumination in Fig. 4b. Light ideality factor ($n_{id,l}$) is determined by $n_{id,l} = \frac{q}{kT} \frac{dV_{oc}}{d \ln(\Phi)}$, where q is the electron charge, k is Boltzmann's constant, T is the absolute temperature, and Φ is the fractional light intensity normalized to one sun. The $n_{id,l}$ values were obtained by fitting linearly to V_{oc} versus log-scaled light intensity data, giving $n_{id,l}$ values of 1.39, 1.81, and 2.30 for PCDTBT1-, PCDTBT-, and PCDTBT8- based devices, respectively. It has been suggested that kT/q approaching unity means less trap-assisted recombination involved in the device operation^[51,52]. Therefore, the smallest $n_{id,l}$ value of PCDTBT1-based device is indicative of the least amount of traps.

By applying the classical Mott-Schottky (M-S) relation, the capacitance-voltage (C - V) characteristics can reveal interfacial charge density, with the charge density being inversely proportional to the straight line slope of the M-S plot^[53]. As shown in Fig. 4c, the slope of the PCDTBT1-based device (4.6×10^{17}) is larger than that of PCDTBT- (3.4×10^{17}) and PCDTBT8- (2.9×10^{17}) based devices, suggesting a lower interfacial charge density. That is to say, charge

accumulation at the perovskite/PCDTBT1 interface is the lowest, which best reduces charge recombination. The recombination process can be clearly reflected through the open-circuit photovoltage decay (OCVD) measurements shown in Fig. 4d. For the OCVD test, the devices were illuminated at open-circuit for a period of time to achieve the photostationary state, and the photocarriers underwent rapid recombination when the light was instantaneously switched off^[49,54]. We monitored the V_{oc} as the function of time during the whole process, and observed that the PCDTBT1-based device showed a much lower decay than the PCDTBT- and PCDTBT8- based devices, and the PCDTBT1-based device had the minimal voltage decay amplitude in the first 5 ms (see the inset of Fig. 4d), which is again consistent with the a lowest charge recombination rate when incorporating PCDTBT1 as HTM.

Electrochemical impedance spectroscopy (EIS) measurements were further carried out to provide information about the internal electrical characteristics under one sun illumination in the frequency range from 1 MHz to 100 Hz. We can gain more insight into the recombination kinetics of our PSC devices through fitting the Nyquist plots displayed in Fig. S6 (Supporting information). Two distinct regions are exhibited in the curves, including a high frequency region representing the charge recombination process and a low frequency region that appears below a frequency of a few hundred Hz, which correlates with slow dielectric and ionic relaxations in perovskite films^[53]. The equivalent circuit model displayed as the inset in Fig. 4e was used for data fitting, in which R_s and R_{rec} are series and recombination resistances respectively, and the fitting results are summarized in Fig. S7 (Supporting information) and Fig. 4e. We found that the R_s extracted from fitting of the EIS spectra are similar, all at around 60 Ω , and the R_{rec} of PCDTBT1-based device is larger than those of the PCDTBT- and PCDTBT8- based devices independent of the applied voltage, which indicates the most reduced recombination rate in its PSC device, and is consistent with the device efficiency results. This could be a result of the decreased trap density at the perovskite/PCDTBT1 interface compared to the PCDTBT-based counterpart and the largest concentration of recombination centers in the PCDTBT8-based device. Therefore we quantitatively calculated the trap density variation of the device through fabricating hole-only devices with the architecture shown in the inset of Fig. 4f. The trap density can be determined by the trap-filled limit voltage (V_{TFL}) using $V_{TFL} = e n_t L^2 / 2 \epsilon \epsilon_0$, where L is the thickness of the perovskite film, ϵ is the relative dielectric constant of MAPbI₃ (taken as 32 from previous reports), and ϵ_0 is the vacuum permittivity (8.854×10^{-12} F m⁻¹)^[35,55]. The trap density n_t of PCDTBT1-based device is calculated to be 1.16×10^{16} cm⁻³. For comparison, the calculated hole trap density of the PCDTBT- and PCDTBT8- based devices are higher at 1.50×10^{16} cm⁻³ and 2.82×10^{16} cm⁻³ respectively, which again confirms the minimum interfacial charge recombination in the PCDTBT1-based device.

The thiophene units in the backbone of these conjugated polymer HTMs have been found to act as Lewis bases to coordinate with the under-coordinated Pb atoms through the electron donating sulfur atoms, and therefore partially passivate the trap states on the perovskite crystal surfaces^[56]. However, we believe that the methoxy side-chains grafted on the BT units of PCDTBT1 can also act as Lewis bases to further passivate trap states through the electron-donating oxygen atoms in the methoxy units. As the computed ESP profiles showed, the O atom can also concentrate negative charges. Therefore, the defect-caused trapping and recombination of charge carriers will be dramatically suppressed at the interface between perovskite and PCDTBT1, and the PCDTBT1-based PSC showed the highest V_{oc} and FF in comparison to the other two devices. Meanwhile, face-on π - π stacks in the PCDTBT1 layer can be retained to some extent as a result of the relatively small dihedral angles in the backbone of PCDTBT1 which has short methoxy side-chains, thus having a limited effect on hole transport via the deterioration of molecular order. Our observation here is consistent with a number of literature reports employing small molecules as HTMs. For instance, a series of anthra[1,2-b:4,3-b':5,6-b'':8,7-b''']tetrathiophene (ATT) based small molecules were designed as HTMs for PSCs, and showed that the HTM using the methoxy unit (-OCH₃) as side chain lead to the best device efficiency exceeding 18% compared with HTMs using butoxy-, hexoxy-, or decoxy- substituents^[57]. Small molecules with *o*-OMe substituents improved device performance more than spiro-OMeTAD which has *p*-OMe substituents^[58]. Another work demonstrated that the charge extraction and recombination behaviors of PSCs could be improved by increasing the number of methoxy units in the triarylamine derivative (TPAC) HTMs^[59].

For comparison, the PCDTBT8 with long octyloxy side-chains showed a poor polarized structure, which may hamper the thiophene interaction with the under-coordinated Pb atoms, resulting in increased defect density at the interface relative to that of PCDTBT. In addition, these long side-chains caused the most destruction of co-planarity to reduce the molecular π - π stacking order due to the steric hindrance effect, hence holes accumulated at the perovskite/PCDTBT8 interface which were not transported quickly can also lead to serious recombination. The defect passivation effect depends critically on the type of side-chains grafted on both small- and macro-molecule backbones, with the methoxy unit having a favorable impact of passivating defects without annihilating the structural ordering in the solid state HTM layers to substantially affect hole transport. Furthermore, the strong interfacial interaction through S-I or S-Pb bonding should also be favorable factors^[60,61], which is effective when employing all three HTMs in this work.

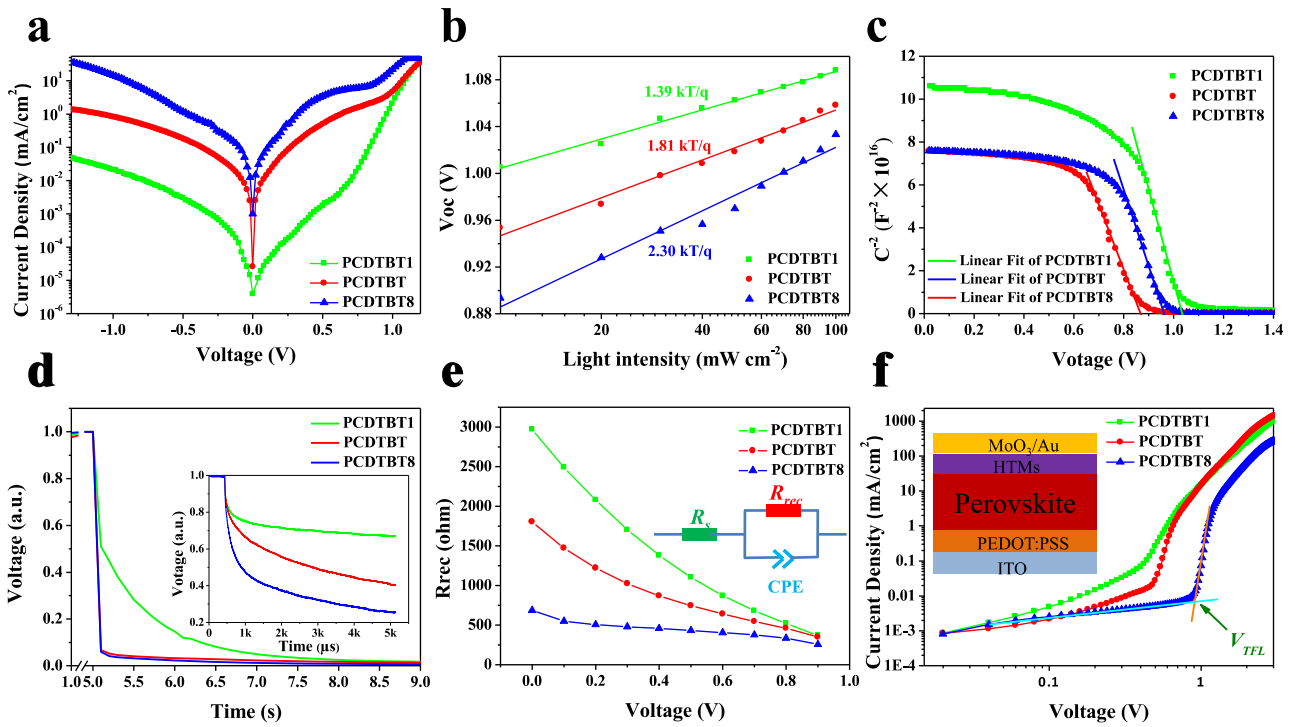


Fig. 4. (a) Dark current density-voltage curve, (b) V_{oc} as a function of light intensity in a semi-log plot, (c) Mott-Schottky (M-S) plots at 10 KHz, (d) open-circuit voltage decay, and (e) R_{rec} obtained from fitting the Nyquist plots through equivalent circuit in the inset, for PSCs incorporating different HTMs. The inset of part (d) represents the photovoltage decaying process in the first 5 ms. (f) Dark current-voltage curves from hole-only devices with the structure shown in the inset.

The Fig. S8 (Supporting information) shows that our conjugated HTM films have much higher water contact angles ($\sim 100^\circ$) than that of spiro-OMeTAD ($\sim 70^\circ$), suggesting great hydrophobicity to better exclude water incursion. We kept the perovskite as well as perovskite/HTM films in ambient conditions with humidity between 40-70%, and present photographs of the films after different aging time in the Fig. S9 (Supporting information). The perovskite/HTM films showed negligible color changes compared to the pristine perovskite film, whilst the perovskite/spiro-OMeTAD film changed from brown to light yellow indicating it underwent irreversible degradation. Accordingly, the decomposition process can be traced through the corresponding X-ray diffraction (XRD) results shown in the Fig. 5a. A weak diffraction peak associated with PbI_2 residues in the perovskite is present in the spectrum of freshly prepared perovskite, which has been commonly observed in the literature due to its two-step preparation process. After an aging time of 15 days in ambient conditions, the diffraction peaks at 2θ of 14.2° , 28.4° (corresponding to characteristic perovskite crystals) for the perovskite without a capping HTM layer and that capped with the spiro-OMeTAD HTM, almost disappeared whilst the intensity of the PbI_2 peak became much stronger. This implies the serious moisture-induced decomposition of perovskite crystals. In contrast, the perovskite diffraction peaks remain almost unchanged when the perovskite was covered by

PCDTBT and PCDTBT1, as a result of effective suppression of the decomposition process. However, the intensities of the perovskite and PbI_2 diffraction peaks reduced and enhanced respectively when the perovskite was capped with PCDTBT8, which means a faster degradation process. Keeping the similar surface hydrophobicity of three conjugated polymers in mind, we attribute this to the different amount of defects existing in these devices, which are susceptible to water and oxygen attacks due to their high degree of activity^[62]. The passivation effects from the thiophene and methoxy units in PCDTBT and PCDTBT1 certainly contribute to reduce the amount of defects in the corresponding PSCs, and help to achieve a higher efficiency as well as longer storage stability.

Finally, we studied the storage lifetime of PSCs employing different HTMs. The epoxy-encapsulated devices were stored in the dark when they were not being tested during this long-term measurement cycle to preclude photo/thermo-induced degradation, thus mainly focusing on the effects of internal trap density on the device stability. The relative humidity in our lab varied between 40-70 % and the ambient temperature varied between 25 to 35 °C. As shown in Fig. 5b, the PCDTBT- and PCDTBT1- based devices show remarkable stability, maintaining 90% of their original PCEs after storage of more than 30 days. This is attributed to their hydrophobic nature compared to that of spiro-OMeTAD. The PCDTBT8-based device shows the worst stability, even though PCDTBT8 is hydrophobic, and this seriously deteriorated device efficiency can be explained by its decomposition shown in Fig. 5a that is mediated by the traps.

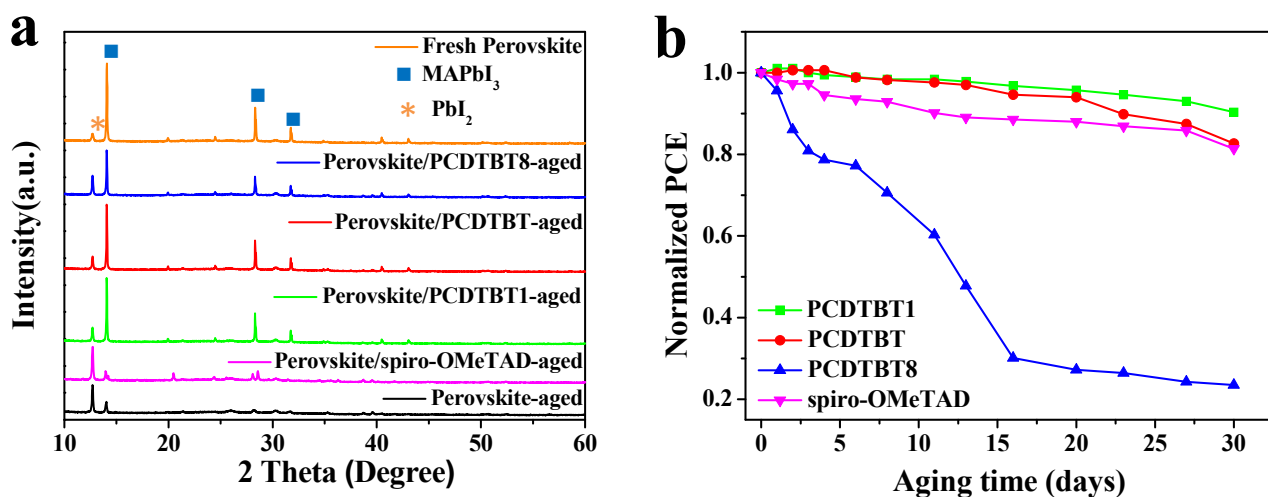


Fig. 5. (a) XRD patterns of perovskite, perovskite/spiro-OMeTAD, perovskite/PCDTBT1, perovskite/PCDTBT and perovskite/PCDTBT8, after exposure to ambient conditions for 15 days (40~70 RH%). (b) The evolution of PCEs for epoxy-encapsulated devices incorporating different HTMs that have been stored under ambient for a duration of 30 days.

In conclusion, we have fabricated PSC devices with an n-i-p structure incorporating dopant-free conjugated polymers as hole transport materials. We demonstrated that the ordered π - π stacking

structure can facilitate charge carrier transport, and the flanked methoxy and octyloxy groups have significant but different impacts on reduce the trap-mediated recombination in PSC devices. A superior performance of 19.1% was achieved using PCDTBT1 as the HTM, its success attributed to the more effective suppression of charge recombination at the perovskite/PCDTBT1 interface by coupling the passivation effect from the thiophene and methoxy units. The storage lifetime of this device is also superior, due to its hydrophobic surface that prevents water penetration, as well as the lower density of trap sites. We note that such a high PCE was achieved by using the simplest perovskite composition of MAPbI₃, and further component engineering of the perovskite could result in perovskite devices with higher photovoltaic performance.

3. Experimental Section

3.1 Materials

The synthetic details of methylammonium iodide (CH₃NH₃I or MAI) and titanium dioxide (TiO₂) solution can be found in a previous work^[Error! Bookmark not defined.]. Lead (II) iodide (PbI₂, 99.9%) was purchased from You Xuan Ltd. Phenyl-C60-butyric acid methyl ester (PC₆₀BM) and 2,2',7,7'-tetrakis(*N,N*-di-*p*-methoxyphenylamine)-9,9'-spirobifluorene (Spiro-OMeTAD) were purchased from Luminescence Technology. Bis(trifluoromethane)sulfonimide lithium salt(Li-TFSI) and 4-*tert*-butylpyridine (TBP) were purchased from Sigma-Aldrich. PCDTBT, PCDTBT1 and PCDTBT8 were synthesized according to our previous reported work. PCDTBT, PCDTBT1 and PCDTBT8 had molecular weights (M_w) and polydispersities (PDI) of 26.5 kDa and 2.18, 57.3 kDa and 2.02, 54.1 kDa and 2.16 respectively.

3.2 Device fabrication

The patterned ITO glass (resistance *ca.* 15Ω sq⁻¹) was cleaned by ultrasonication sequentially in water, ethanol, and isopropyl alcohol for 10 min. each, then further treated with ultraviolet-ozone for 10 min to remove organic contaminants. The details of spiro-OMeTAD based device including TiO₂ film, PCBM film, MAPbI₃ film, spiro-OMeTAD film and Au cathode deposition are detailed in our previous report^[35]. For the PCDTBT, PCDTBT1 and PCDTBT8 based devices, the HTMs were formed by spin coating their solution (5 mg/ml in chlorobenzene) at 2000 rpm for 30 s. Finally, 10-nm-thick molybdenum oxide and 80-nm-thick gold electrodes were deposited on the top of the devices for PCDTBT, PCDTBT1 and PCDTBT8 based devices through a metal shadow mask by thermal evaporation at the vacuum level of 10⁻⁷ Torr. The active area for all solar cells was 0.04 cm² defined by the shadow mask.

4.3 Characterization

The density functional theory (DFT) method and Gaussian 09 package were used to simulate electrostatic potential (ESP) distribution and dihedral angles in these conjugated polymers. To

simplify the calculation, the octyl groups in the carbazole moiety were replaced with CH₃ groups. X-ray diffraction spectra were measured with an X-ray diffractometer (D8 Advance, Bruker, Germany) using Cu K α radiation at 40 kV and 40 mA. The surface morphology was characterized by SPM (NT-MDT, Russian). The steady-state photoluminescence (PL) spectra were obtained using a PL microscopic spectrometer (Flex One, Zolix, China), the excitation source of PL utilizes a 532 nm CW laser. Time-resolved PL decay was measured using a Delta Flex Fluorescence Lifetime System monitored at 770 nm. Impedance measurements were measured using the ModuLab XM electrochemical workstation (AMETEK, UK) under a series of voltages with the amplitude of 10 mV from 1 MHz to 100 Hz under one AM 1.5G illumination conditions. Equivalent circuit simulations were conducted using the software package ZView (Scribner Associate, Inc.). Capacitance-voltage and open-circuit photovoltage decay measurements were also obtained by the ModuLab XM electrochemical workstation (AMETEK, UK). External quantum efficiency (EQE) was measured with an EQE system (Zolix, China) equipped with a standard Si diode. The monochromatic beam was generated from a 150 W xenon lamp. The current density-voltage (*J-V*) curves of the devices were measured in ambient air under simulated sunlight (100 mW cm⁻²) using a Newport 3A solar simulator, with light intensity was calibrated with silicon solar cell certified by the National Renewable Energy Laboratory (NREL). *J-V* characteristics were recorded using *J-V* sweep software developed by Ossila Ltd. (Sheffield, UK) and a Keithley 2612B source meter unit. The devices were masked with a metal aperture mask to accurately define a test area of 2.12 mm² on each pixel and to eliminate the influence of any edge effects. The stabilized power output versus time of devices was measured by holding a bias near the maximum power output point at the same conditions.

Acknowledgements

We thank Prof. David Lidzey (University of Sheffield) for helpful discussion. T.W. acknowledges funding supports from the National Natural Science Foundation of China (21504065, 21774097), the Fundamental Research Funds for the Central Universities (WUT: 2015III018 and 2015III029) of China, and the Recruitment Program of Global Experts (1000 Talents Plan) of China. H.Y. and A.I. thank financial support from EPSRC via grant EP/I028641/1.

References

-
- [1] W. S. Yang, J. H. Noh, N. J. Jeon, Y. C. Kim, S. Ryu, J. Seo, S. I. Seok, *Science* 348 (2015) 1234-1237.
 - [2] G. Xing, N. Mathews, S. Sun, S. S. Lim, Y. M. Lam, M. Grätzel, S. Mhaisalkar, T. C. Sum, *Science* 342 (2013) 344-347.
 - [3] L. Yang, A. T. Barrows, D. G. Lidzey, T. Wang, *Rep. Prog. Phys.* 79 (2016) 26501.
 - [4] A. Kojima, K. Teshima, Y. Shirai, T. Miyasaka, *J. Am. Chem. Soc.* 131 (2009) 6050-6051.

-
- [5] W. S. Yang, B. W. Park, E. H. Jung, N. J. Jeon, Y. C. Kim. *Science* 356 (2017), 1376-1379.
- [6] M. Saliba, T. Matsui, J. Y. Seo, K. Domanski, J. P. Correa-Baena, M. K. Nazeeruddin, S. M. Zakeeruddin, W. Tress, A. Abate, A. Hagfeldt, M. Grätzel, *Energy Environ. Sci.* 9 (2016) 1989-1997.
- [7] M. Saliba, T. Matsui, K. Domanski, J. Y. Seo, A. Ummadisingu, S. M. Zakeeruddin, J. P. Correa-Baena, W. R. Tress, A. Abate, A. Hagfeldt, M. Grätzel, *Science* 354 (2016) 206-209.
- [8] M. Saliba, S. Orlandi, T. Matsui, S. Aghazada, M. Cavazzini, J. Correa-Baena, P. Gao, R. Scopelliti, E. Mosconi, K. Dahmen, F. De Angelis, A. Abate, A. Hagfeldt, G. Pozzi, M. Grätzel, M. K. Nazeeruddin, *Nat. Energy* 1 (2016) 15017.
- [9] J. You, L. Meng, T. Song, T. Guo, Y. M. Yang, W. Chang, Z. Hong, H. Chen, H. Zhou, Q. Chen, Y. Liu, N. De Marco, Y. Yang, *Nat. Nanotechnol.* 11 (2015) 75-81.
- [10] H. Zhou, Q. Chen, G. Li, S. Luo, T. B. Song, H. S. Duan, Z. Hong, J. You, Y. Liu, Y. Yang, *Science* 345 (2014) 542-546.
- [11] X. Zheng, B. Chen, J. Dai, Y. Fang, Y. Bai, Y. Lin, H. Wei, X. C. Zeng, J. Huang, *Nat. Energy* 2 (2017) 17102.
- [12] L. Calió, S. Kazim, M. Grätzel, S. Ahmad, *Angew. Chem.* 55 (2016) 14522-14545.
- [13] D. Bi, W. Tress, M. I. Dar, P. Gao, J. Luo, C. Renevier, K. Schenk, A. Abate, F. Giordano, J. P. Correa Baena, J. D. Decoppet, S. M. Zakeeruddin, M. K. Nazeeruddin, M. Grätzel, A. Hagfeldt, *Science Advances* 2 (2016) e1501170.
- [14] D. Son, J. Lee, Y. J. Choi, I. Jang, S. Lee, P. J. Yoo, H. Shin, N. Ahn, M. Choi, D. Kim, N. Park, *Nat. Energy* 1 (2016) 16081.
- [15] X. Li, D. Bi, C. Yi, J. D. Decoppet, J. Luo, S. M. Zakeeruddin, A. Hagfeldt, M. Grätzel, *Science* 353 (2016) 58-62.
- [16] A. Abate, T. Leijtens, S. Pathak, J. Teuscher, R. Avolio, M. E. Errico, J. Kirkpatrick, J. M. Ball, P. Docampo, I. McPherson, H. J. Snaith, *Phys. Chem. Chem. Phys.* 15 (2013) 2572.
- [17] U. B. Cappel, T. Daeneke, U. Bach, *Nano Lett.* 12 (2012) 4925-4931.
- [18] Y. Yue, N. Salim, Y. Wu, X. Yang, A. Islam, W. Chen, J. Liu, E. Bi, F. Xie, M. Cai, L. Han, *Adv. Mater.* 28 (2016) 10738-10743.
- [19] A. D. Sheikh, A. Bera, M. A. Haque, R. B. Rakhi, S. D. Gobbo, H. N. Alshareef, T. Wu, *Sol. Energ. Mat. Sol. C.* 137 (2015) 6-14.
- [20] Q. Chen, H. Zhou, T. Song, S. Luo, Z. Hong, H. Duan, L. Dou, Y. Liu, Y. Yang, *Nano Lett.* 14 (2014) 4158-4163.
- [21] H. Yu, H. Lu, F. Xie, S. Zhou, N. Zhao, *Adv. Funct. Mater.* 26 (2016) 1411-1419.
- [22] M. L. Agiorgousis, Y. Sun, H. Zeng, S. Zhang, *J. Am. Chem. Soc.* 136 (2014) 14570-14575.
- [23] N. K. Noel, A. Abate, S. D. Stranks, E. S. Parrott, V. M. Burlakov, A. Goriely, H. J. Snaith, *Acs Nano* 8 (2014) 9815-9821.
- [24] S. M. Jain, Z. Qiu, L. Häggman, M. Mirmohades, M. B. Johansson, T. Edvinsson, G. Boschloo, *Energy Environ. Sci.* 9 (2016) 3770-3782.
- [25] F. Wang, W. Geng, Y. Zhou, H. Fang, C. Tong, M. A. Loi, L. Liu, N. Zhao, *Adv. Mater.* 28 (2016) 9986-9992.
- [26] Y. Lin, L. Shen, J. Dai, Y. Deng, Y. Wu, Y. Bai, X. Zheng, J. Wang, Y. Fang, H. Wei, W. Ma, X. C. Zeng, X. Zhan, J. Huang, *Adv. Mater.* 29 (2017) 1604545.
- [27] P. Qin, S. Tanaka, S. Ito, N. Tetreault, K. Manabe, H. Nishino, M. K. Nazeeruddin, M. Grätzel, *Nat. Commun.* 5 (2014) 3834.
- [28] J. A. Christians, R. C. Fung, P. V. Kamat, *J. Am. Chem. Soc.* 136 (2013) 758-764.
- [29] F. Zhang, X. Yang, M. Cheng, W. Wang, L. Sun, *Nano Energy* 20 (2016) 108-116.
- [30] L. Yang, F. Cai, Y. Yan, J. Li, D. Liu, A. J. Pearson, T. Wang, *Adv. Funct. Mater.* (2017) 1702613.

-
- [31] J. H. Heo, S. H. Im, J. H. Noh, T. N. Mandal, C. Lim, J. A. Chang, Y. H. Lee, H. Kim, A. Sarkar, M. K. Nazeeruddin, M. Grätzel, S. I. Seok, *Nat. Photonics* 7 (2013) 486-491.
- [32] M. Ahmadi, Y. Hsiao, T. Wu, Q. Liu, W. Qin, B. Hu, *Adv. Energy Mater.* 7 (2017) 1601575.
- [33] H. Chen, W. Fu, C. Huang, Z. Zhang, S. Li, F. Ding, M. Shi, C. Li, A. K. Y. Jen, H. Chen, *Adv. Energy Mater.* (2017) 1700012.
- [34] J. Hua, X. Li, M. Cai, Z. Zhou, K. Yun, F. Xie, Z. Lan, J. Hua, L. Han, *J. Mater. Chem. A* 5 (2017) 10480-10485.
- [35] F. Cai, L. Yang, Y. Yan, J. Zhang, F. Qin, D. Liu, Y. Cheng, Y. Zhou, T. Wang, *J. Mater. Chem. A* 5 (2017) 9402-9411.
- [36] T. Wang, N. W. Scarratt, H. Yi, I. F. Coleman, Y. Zhang, R. T. Grant, J. Yao, M. W. A. Skoda, A. D. F. Dunbar, R. A. L. Jones, A. Iraqi, D. G. Lidzey, *J. Mater. Chem. C* 3 (2015) 4007-4015.
- [37] H. Yi, S. Al-Faifi, A. Iraqi, D. C. Watters, J. Kingsley, D. G. Lidzey, *J. Mater. Chem.* 21 (2011) 13649.
- [38] T. Wang, N. W. Scarratt, H. Yi, A. D. F. Dunbar, A. J. Pearson, D. C. Watters, T. S. Glen, A. C. Brook, J. Kingsley, A. R. Buckley, M. W. A. Skoda, A. M. Donald, R. A. L. Jones, A. Iraqi, D. G. Lidzey, *Adv. Energy Mater.* 3 (2013) 505-512
- [39] H. J. Snaith, A. Abate, J. M. Ball, G. E. Eperon, T. Leijtens, N. K. Noel, S. D. Stranks, J. T. Wang, K. Wojciechowski, W. Zhang, *J. Phys. Chem. Lett.* 5 (2014) 1511-1515.
- [40] E. L. Unger, E. T. Hoke, C. D. Bailie, W. H. Nguyen, A. R. Bowring, T. Heumüller, M. G. Christoforo, M. D. McGehee, *Energy Environ. Sci.* 7 (2014) 3690-3698.
- [41] W. Tress, N. Marinova, T. Moehl, S. M. Zakeeruddin, M. K. Nazeeruddin, M. Grätzel, *Energy Environ. Sci.* 8 (2015) 995-1004.
- [42] W. Li, Y. Yan, Y. Gong, J. Cai, F. Cai, R. S. Gurney, D. Liu, A. J. Pearson, D. G. Lidzey, T. Wang, *Adv. Funct. Mater.* 28 (2018) 1704212.
- [43] S. D. Stranks, G. E. Eperon, G. Grancini, C. Menelaou, M. J. P. Alcocer, T. Leijtens, L. M. Herz, A. Petrozza, H. J. Snaith, *Science* 342 (2013) 341-344.
- [44] T. Wang, A. J. Pearson, A. D. F. Dunbar, P. A. Staniec, D. C. Watters, H. Yi, A. J. Ryan, R. A. L. Jones, A. Iraqi, D. G. Lidzey, *Adv. Funct. Mater.* 22 (2012) 1399-1408.
- [45] P. A. Staniec, A. J. Parnell, A. D. F. Dunbar, H. Yi, A. J. Pearson, T. Wang, P. E. Hopkinson, C. Kinane, R. M. Dalgliesh, A. M. Donald, A. J. Ryan, A. Iraqi, R. A. L. Jones, D. G. Lidzey, *Adv. Energy Mater.* 1 (2011) 499-504.
- [46] M. Wongstringer, J. E. Bishop, J. A. Smith, D. K. Mohamad, A. J. Parnell, V. Kumar, C. Rodenburgh, D. G. Lidzey, *J. Mater. Chem. A* 5 (2017) 15714-15723.
- [47] J. M. Szarko, J. Guo, Y. Liang, B. Lee, B. S. Rolczynski, J. Strzalka, T. Xu, S. Loser, T. J. Marks, L. Yu, L. X. Chen, *Adv. Mater.* 22 (2010) 5468-5472.
- [48] H. Zhou, L. Yang, S. Xiao, S. Liu, W. You, *Macromolecules* 43 (2010) 811-820.
- [49] K. Chen, Q. Hu, T. Liu, L. Zhao, D. Luo, J. Wu, Y. Zhang, W. Zhang, F. Liu, T. P. Russell, R. Zhu, Q. Gong, *Adv. Mater.* 28 (2016) 10718-10724.
- [50] Q. Wang, Y. Shao, Q. Dong, Z. Xiao, Y. Yuan, *Energy Environ. Sci.* 7 (2014) 2359-2365.
- [51] S. R. Cowan, A. Roy, A. J. Heeger, *Phys. Rev. B* 82 (2010) 245207.
- [52] G. A. H. Wetzelaer, M. Scheepers, A. M. Sempere, C. Momblona, J. Ávila, H. J. Bolink, *Adv. Mater.* 27 (2015) 1837-1841.
- [53] Y. Liu, M. Bag, L. A. Renne, Z. A. Page, P. Kim, T. Emrick, D. Venkataraman, T. P. Russell, *Adv. Energy Mater.* 6 (2016) 1501606.

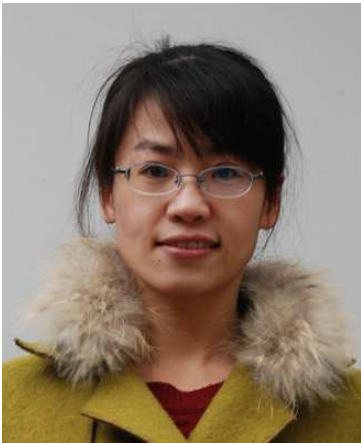
-
- [54] A. Pockett, G. E. Eperon, T. Peltola, H. J. Snaith, A. Walker, L. M. Peter, P. J. Cameron, *J. Phys. Chem. C* 119 (2015) 3456-3465.
- [55] Q. Dong, Y. Fang, Y. Shao, P. Mulligan, J. Qiu, L. Cao, J. Huang, *Science* 347 (2015) 967-970.
- [56] C. Zhang, M. Li, Z. Wang, Y. Jiang, H. Liu, Y. Yang, X. Gao, H. Ma, *J. Mater. Chem. A* 5 (2017) 2572-2579.
- [57] I. Zimmermann, J. Urieta-Mora, P. Gratia, J. Aragón, G. Grancini, A. Molina-Ontoria, E. Ortí, N. Martín, M. K. Nazeeruddin, *Adv. Energy Mater.* 7 (2017) 1601674.
- [58] N. J. Jeon, H. G. Lee, Y. C. Kim, J. Seo, J. H. Noh, J. Lee, S. I. Seok, *J. Am. Chem. Soc.* 136 (2014) 7837-7840.
- [59] S. J. Park, S. H. Jeon, I. K. Lee, J. Zhang, H. Jeong, J. Y. Park, J. Bang, T. K. Ahn, H. W. Shin, B. G. Kim, H. J. Park, *J. Mater. Chem. A* 5 (2017) 13220-13227.
- [60] N. Wang, K. Zhao, T. Ding, W. Liu, A. S. Ahmed, Z. Wang, M. Tian, X. W. Sun, Q. Zhang, *Adv. Energy Mater.* (2017) 1700522.
- [61] H. Chen, W. Fu, C. Huang, Z. Zhang, S. Li, F. Ding, M. Shi, C. Li, A. K. Y. Jen, H. Chen, *Adv. Energy Mater.* (2017) 1700012.
- [62] Q. Wang, B. Chen, Y. Liu, Y. Deng, Y. Bai, Q. Dong, J. Huang, *Energy Environ. Sci.* 10 (2017) 516-522.



Feilong Cai was born in 1993. He received a B.S. degree in Polymer Materials and Engineering from Wuhan University of Technology in 2015. He is currently an M.S. student working on photovoltaics, with a specific focus on various electron/hole transport materials.



Jinlong Cai was born in 1994 in Nantong, China. He received a B.S. degree in Polymer Materials and Engineering from Hubei University of Technology in 2016. He is currently an M.S. student working on organic photovoltaics.



Liyan Yang comes from Zhejiang province. She received a Bachelor degree in Management from Wuhan College of International Business and Economics in 2009 and a Master degree in Textile Materials from Donghua University in 2012. She is currently a Ph.D. student and her research concerns improving the power conversion efficiency of perovskite solar cells via morphology modification and interface engineering.



Wei Li was born in 1992. He received a B.S. degree in Materials science and Engineering from Jinan University in 2013 and an M.S. degree in Materials Science and Engineering from Wuhan University of Technology in 2016. He is currently a Ph.D. candidate with a specific focus on polymer solar cells.



Dr. Robert Gurney received his Ph.D. in Physics from the University of Surrey in 2013 under the supervision of Professor Joe Keddie. He spent a further 6 months in the same group as a post-doc, working with industrial partners on moisture analysis and scanning probe microscopy of polymer films, before moving to ESPCI in Paris. There, he worked on the adhesion and rheology of SBR at short time scales with Profs. Costantino Creton and Anke Lindner, collaborating with Michelin. He joined the group at Wuhan University of Technology in May 2017 as a post-doc to study optoelectronic devices.



Dr. Hunan Yi received his MSc from Shanghai China, and his PhD from University of St Andrews on Dye-Sensitised Solar Cells, where he remained as a research fellow after Ph.D. until 2004. He then became a postdoctoral research associate at the University of Sheffield, developing various conjugated polymers for organic solar cell applications. Since 2015, he is a Knowledge Transfer Account (KTA) associate with both the University of Sheffield and Ossila Ltd. UK.



Dr. Ahmed Iraqi obtained his BSc from the University of Fes (Morocco) in 1984. This was followed by an MSc in Chemistry from University Paul Sabatier in Toulouse in 1985 and a Ph.D. from the same institution in 1988. Until 1996 he was a Postdoctoral Research Associate at the University of St Andrews, when he became a Lecturer at Lancaster University. In 2000 he was appointed Lecturer at the University of Sheffield, where he was promoted to Senior Lecturer in 2009 and Reader in 2013.



Dr. Dan Liu studied soft condensed matter physics in the University of Surrey since Oct. 2006, and was awarded a PhD in Jun. 2010. From Nov. 2010 to Aug. 2012, she was a post-doc research associate in the school of physics and astronomy, University of Leeds, working on lipid membrane. In 2013, Dan was awarded the "ChuTian" Scholar of Hubei province (China), and was appointed associate professor in the school of materials science & engineering at Wuhan University of Technology, China. Her research interests include soft matter physics and polymer materials.



Prof. Tao Wang received a B.S. in Polymer Materials (2002) and an M.S. in Materials Science (2005). He obtained his Ph.D. in Physics from the University of Surrey (UK) in Feb. 2009. He then took a post-doc position in the same group until Oct. 2009 when he moved to the University of Sheffield (UK), where he worked with Prof. Richard Jones, FRS and Prof. David Lidzey on organic solar cells. He was awarded funding from “Recruitment Program of Global Experts” of China in 2013 and was appointed professor in Wuhan University of Technology (China). His research interests are optoelectronic devices, polymer physics and polymer materials.